Iterated triangle partitions

Steve Butler*† Ron Graham‡

Abstract

For a given triangle there are many points associated with the triangle that lie in its interior; examples include the incenter (which can be found by the intersection of the angle bisectors) and the centroid (which can be found by the intersection of the medians). Using this point one can naturally subdivide the triangle into either three or six "daughter" triangles. We can then repeat the same process on each of the daughters and so on and so on. A natural question is after some large number of steps what does a typical nth generation daughter look like (up to similarity)? In this paper we look at this problem for both the incenter and the centroid and show that they have very distinct behavior as n gets large. We will also look at the Gergonne point and the Lemoine point.

1 Introduction

In this paper we will be considering triangles and are concerned only with the shape, i.e., up to similarity. So we can denote a triangle T by the triple $T(A, B, C)$ where A, B and C are the interior angles. Given a point P in the interior of T we can use the point to subdivide T into smaller "daughter" triangles. This is done by taking each vertex and drawing the line passing through P and connecting it to the opposite side (sometimes referred to as Cevians), subdividing the triangle into six daughters (Figure 1a); or by taking each vertex and drawing the line to P subdividing into three daughters (Figure 1b).

(a) Six daughters. (b) Three daughters.

Figure 1: Given an interior point P how to subdivide the triangle.

*Department of Mathematics, UCLA, Los Angeles, CA 90095 (butler@math.ucla.edu).

†This work was partially done with support of an NSF Mathematical Sciences Postdoctoral Fellowship.

‡Department of Computer Science and Engineering, University of California, San Diego, La Jolla, CA 92093 (graham@ucsd.edu).

We are interested in the case when P is a well-defined point lying in the interior of T for any non-degenerate T. Examples of such points include the *incenter* (which is the intersection of the angle bisectors of T), the *centroid* (which is the intersection of the medians of T), along with many others. A rather complete listing of well known distinguished points associated with triangles is maintained at the Encyclopedia of Triangle Centers [9] (however not all of these points will always lie in the interior of T, the excenter being one such example).

Once we have settled on a way of choosing P, we can iterate the process of subdivision, say for n times, producing 6^n (or 3^n) nth generation daughters from our original triangle T. We are interested in what can be said about an nth generation daughter of T as n goes to infinity. For example, what is the distribution of the shape of the daughters? What is the distribution of the smallest angle (or second smallest angle) of T? It will turn out that the answers to these questions depend in a crucial (and currently not well understood) way on exactly how P is chosen. In the following sections, we will specify various choices for P and address these questions and show that well known points P can produce dramatically different results as n goes to infinity.

To help us answer these questions we first will need a convenient way of describing the triangles. Each triangle $T(A, B, C)$ corresponds to a point $(A, B, C) \in \mathbb{E}^3$ which will lie in the intersection of the plane $x + y + z = \pi$ with the positive orthant (see Figure 2). We will denote this intersection, which is actually an equilateral triangle, by P (this representation has been used before in the analysis of pedal triangles; see [1, 10, 11]).

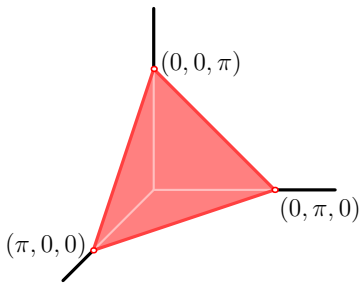

Figure 2: Representing triangles as points in $\mathbb{E}^3$.

2 Subdividing by bisectors

One of the easiest points P to work with is the incenter which is formed by using the angle bisectors. What is nice about this point is that the angles in the daughter triangles are linear combinations of the angles in the original triangle. So the angles of the daughter triangle can be formed via matrix multiplication. This transforms the problem into a Markov process using matrices which has been extensively studied (see the survey [6] for more information). We will consider both possibilities of subdivision shown in Figure 1.

2.1 Subdividing into three daughters

If we associate the triangle $T(A, B, C)$ with the vector $\mathbf{t} = (A, B, C)^*$ in $\mathbb{E}^3$, then the three daughters of T can be found by $M_i\mathbf{t}$ where $i \in \{1, 2, 3\}$ and

$$M_1 = \begin{pmatrix} 1/2 & 0 & 0 \\ 1/2 & 1 & 1/2 \\ 0 & 0 & 1/2 \end{pmatrix}, \qquad M_2 = \begin{pmatrix} 1 & 1/2 & 1/2 \\ 0 & 1/2 & 0 \\ 0 & 0 & 1/2 \end{pmatrix}, \qquad M_3 = \begin{pmatrix} 1/2 & 0 & 0 \\ 0 & 1/2 & 0 \\ 1/2 & 1/2 & 1 \end{pmatrix}.$$

The nth generation daughters of T can then be found by $M_{i_1}M_{i_2}\cdots M_{i_n}\mathbf{t}$ where each $i_j \in \{1, 2, 3\}$. Starting with the triangle $T(\pi/9, 2\pi/9, 2\pi/3)$ we have plotted the nth generation daughters for $n = 2, 4, 6, 8$ in Figure 3.

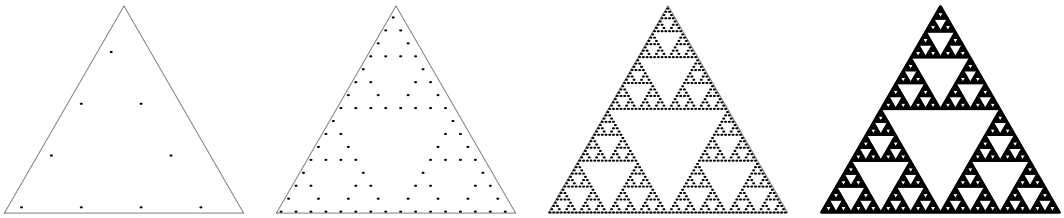

(a) $n = 2$. (b) $n = 4$. (c) $n = 6$. (d) $n = 8$.

Figure 3: The nth generation daughters for angle bisectors with three daughters at each generation.

The figures are very suggestive about what is happening. To see why we are getting the Sierpinski triangle it helps to see how the image of M_i maps P to P. This is shown in Figure 4.

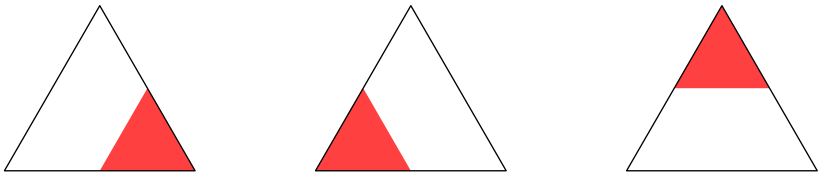

Figure 4: The image of P under the three maps M_i.

So we have that there will be exactly one daughter in each of the subtriangles indicated in Figure 5a. Similarly, if we look at the location of the second generation daughters there will be one daughter in each of the nine triangles indicated in Figure 5b, and if we look at the location of the third generation daughters there will be one daughter in each of the twenty seven triangles indicated in Figure 5c. Since this process mirrors that used to form the Sierpinski triangle, as n goes to infinity the distribution of daughters are the points in the Sierpinski triangle.

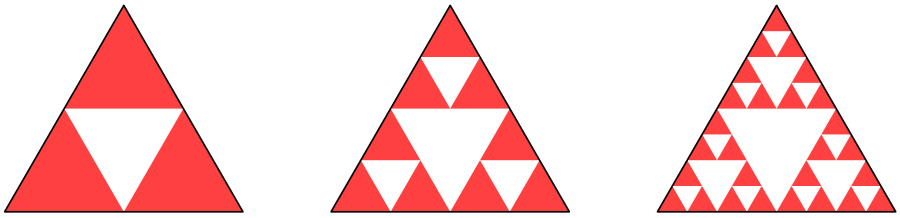

(a) First generation. (b) Second generation. (c) Third generation.

Figure 5: Location of the descendants in the first three generations.

2.2 Dividing into six triangles

As before if we associate a triangle $T(A, B, C)$ with the vector $\mathbf{t} = (A, B, C)^*$ in $\mathbb{E}^3$, then the six daughters of T can be found by $M_i\mathbf{t}$ where $i \in \{1, 2, 3, 4, 5, 6\}$ and

$$M_1 = \begin{pmatrix} 1/2 & 0 & 0 \\ 1/2 & 1/2 & 0 \\ 0 & 1/2 & 1 \end{pmatrix}, \quad M_2 = \begin{pmatrix} 1/2 & 1/2 & 0 \\ 0 & 1/2 & 0 \\ 1/2 & 0 & 1 \end{pmatrix}, \quad M_3 = \begin{pmatrix} 1 & 0 & 1/2 \\ 0 & 1/2 & 0 \\ 0 & 1/2 & 1/2 \end{pmatrix},$$
$$M_4 = \begin{pmatrix} 1 & 1/2 & 0 \\ 0 & 1/2 & 1/2 \\ 0 & 0 & 1/2 \end{pmatrix}, \quad M_5 = \begin{pmatrix} 1/2 & 0 & 1/2 \\ 1/2 & 1 & 0 \\ 0 & 0 & 1/2 \end{pmatrix}, \quad M_6 = \begin{pmatrix} 1/2 & 0 & 0 \\ 0 & 1 & 1/2 \\ 1/2 & 0 & 1/2 \end{pmatrix}.$$

And as before we can form the nth generation daughters by looking at all 6^n possible products of the form $M_{i_1}M_{i_2}\cdots M_{i_n}\mathbf{t}$ with each $i_j \in \{1, 2, 3, 4, 5, 6\}$. Starting with the equilateral triangle $T_1 = T(\pi/3, \pi/3, \pi/3)$ we have plotted the nth generation daughters for $n = 1, 3, 5$ in Figure 6.

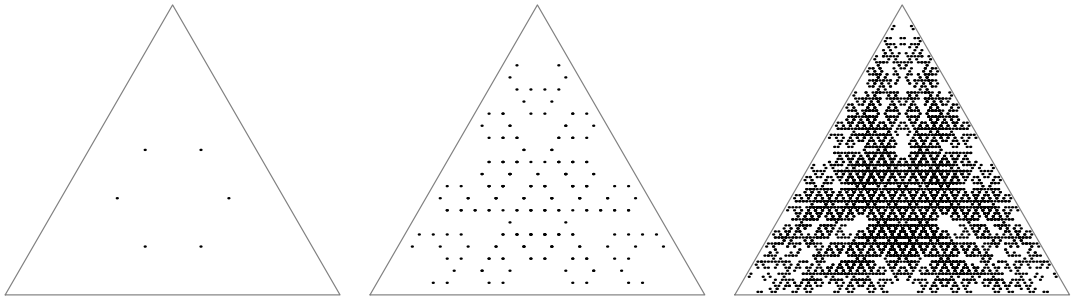

(a) $n = 1$. (b) $n = 3$. (c) $n = 5$.

Figure 6: The nth generation daughters for angle bisectors with six daughters at each generation.

Looking at Figure 6c we see that the daughters seem to fill in P rather uniformly. A patient count though will reveal that there are far fewer than 6^5 triangles in Figure 6c. It is not hard to see that an nth generation daughter of the equilateral triangle must have the form $T(u_1\pi/2^n, u_2\pi/2^n, u_3\pi/2^n)$ for positive integers u_1, u_2, u_3 with $u_1 + u_2 + u_3 = 2^n$. In

particular there are at most $\binom{2^n}{2}$ possible different daughter triangles among the 6^n which will be generated. So on average each triangle is being hit approximately $2(3/2)^n$ times. In particular, any triangle which is not being hit must be missed for a good reason. It is not too hard to see that one condition that is needed is for $\gcd(u_1, u_2, u_3) = 1$, which rules out a positive fraction of the daughters but does not still explain all of the missing daughters.

If we start with a triangle which does not have rational multiples of π then we do not have as many triangles stacking up on top of each other. As an example, the fifth generation daughters of $T_2 = T(\pi/3, \sqrt{2}\pi/3, (2-\sqrt{2})\pi/3)$ are shown in Figure 7 (this should be compared to Figure 6c).

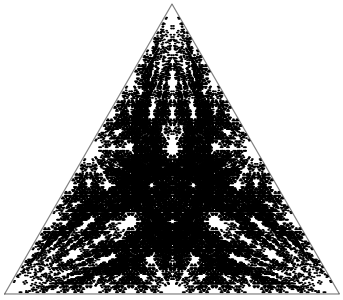

Figure 7: The fifth generation daughters for angle bisectors starting with an "irrational" triangle.

One problem that we run into is that the triangles can be fairly densely packed in these pictures. So instead of plotting the individual triangles it is better to look at a histogram. We will divide P into a large number of small regions and then shade each region according to the number of triangles that fall into that region, the darker a region is the more triangles fall into that region. We have plotted histograms for T_1 and T_2 in Figure 8 (these should be compared with Figures 6c and 7).

The situation is obviously much richer than the previous case when we looked at three daughters. The reason for this is previously the image of each one of the M_i was disjoint, but this is no longer the case. If we plot the images of the six maps we get Figure 9, in particular there is a lot of overlap between pairs of maps.

However, we still have one nice feature of these maps. Namely, they are contracting. To see this we note that we can put P into $\mathbb{E}^2$ by putting $T(A, B, C)$ at $((A + 2B)/\sqrt{3}, A)$. We then can put the first generation daughter $T(A/2, (A+B)/2, (B+2C)/2)$ at $((3A + 2B)/(2\sqrt{3}), A/2)$. If we now compare the distance between triangles $T(A, B, C)$ and $T(A', B', C')$ and their daughters, a calculation shows

$$\frac{3}{4}\left(\left(\frac{A+2B}{\sqrt{3}} - \frac{A'+2B'}{\sqrt{3}}\right)^2 + \left(A - A'\right)^2\right) - \left(\left(\frac{3A+2B}{2\sqrt{3}} - \frac{3A'+2B'}{2\sqrt{3}}\right)^2 + \left(\frac{A}{2} - \frac{A'}{2}\right)^2\right)$$
$$= \frac{2}{3}\left(B - B'\right)^2 \geq 0.$$

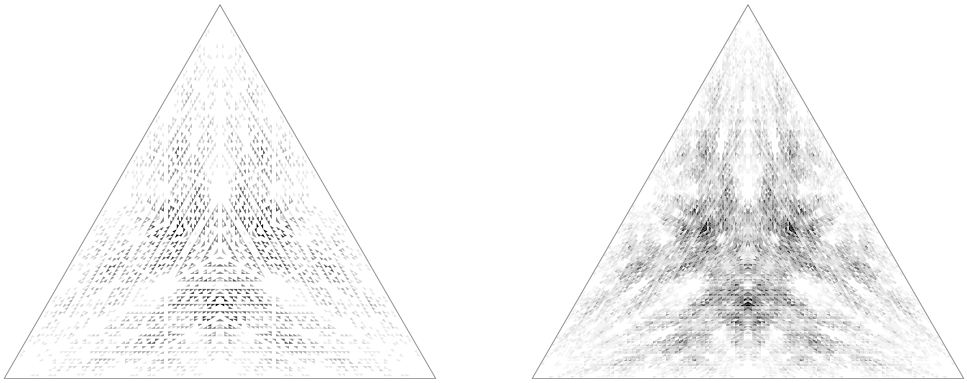

(a) Triangle T_1; $n = 5$.

(b) Triangle T_2; $n = 5$.

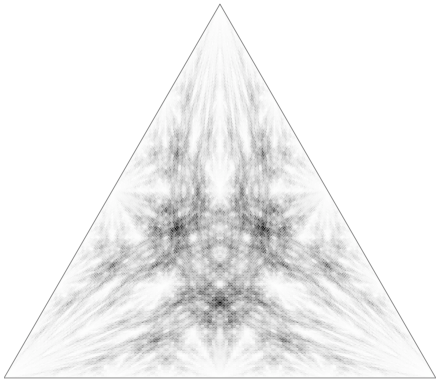

(c) Triangle T_1; $n = 12$.

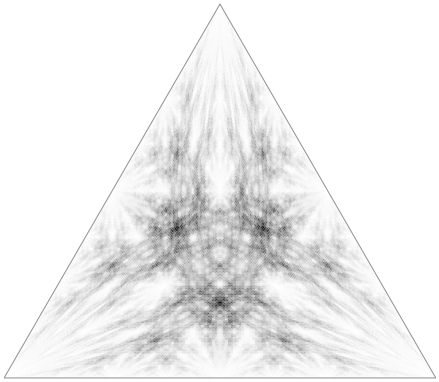

(d) Triangle T_2; $n = 12$.

Figure 8: Histograms for the distribution of triangles in P under bisector division.

It follows that for the euclidean distance d we have

$$d\big(T(A/2,(A+B)/2,(B+2C)/2),T(A'/2,(A'+B')/2,(B'+2C')/2)\big) \\ \leq \frac{\sqrt{3}}{2}d\big(T(A,B,C),T(A',B',C')\big).$$

By symmetry, the same statement holds for all the daughter triangle maps.

Since these maps are contracting with Lipschitz constant $\sqrt{3}/2$ then it follows (see [6]) that there is a fixed stationary distribution on P that the process converges to. Further it converges exponentially. Hence Figures 8c and 8d are nearly identical, and these are approximations for the histogram of the limiting distribution.

2.2.1 The smallest angle

We now consider the problem of analyzing the distributions of the smallest angles. Just as we have a quick rate of convergence to the stationary distribution in P; we experimentally see a quick convergence to the same distribution of minimal angles. In Figure 10 we split

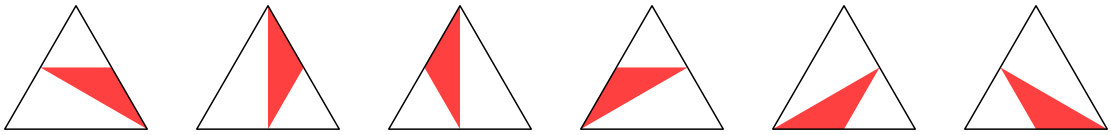

Figure 9: The image of P under the six maps M_i.

the interval between 0 and $\pi/3$ into 1000 intervals and took $50,000,000$ random walks of length 50 in this Markov process and recorded the minimum angle.

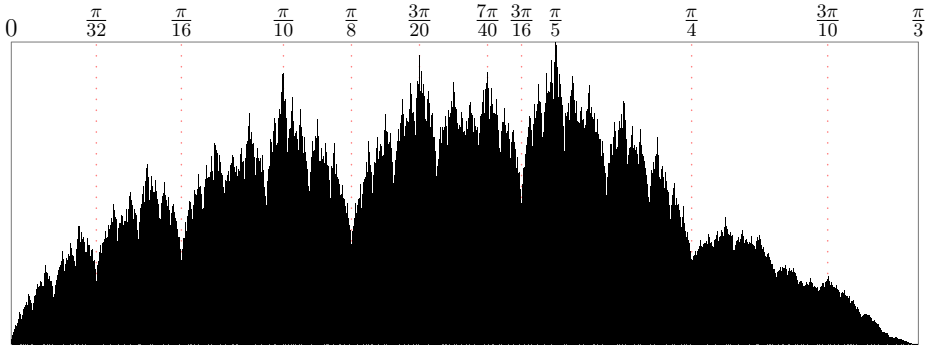

Figure 10: The distribution of the smallest angle using bisectors.

A few things certainly stand out. Perhaps the simplest thing to observe is that the minimum angles are not concentrated near 0, so that the nth generation daughters are not becoming "flat". There also is a certain amount of self-similarity (but given the distributions we saw in Figure 8cd this should not be surprising). We also have marked a few of the values between 0 and $\pi/3$ in Figure 10. In particular we see that a few of the "valleys" are located at $\pi/16, \pi/8, 3\pi/16, \pi/4$ and a few of the peaks are located at $\pi/10, 3\pi/20, 7\pi/40, \pi/5$.

The tallest peak is located at $\pi/5$. If we look closely at the histograms in Figure 8cd we see that the darkest region is located at $T(\pi/5, \pi/5, 2\pi/5)$. This particular triangle has the following unique property; $T(\pi/5, 2\pi/5, 2\pi/5)$ is the only triangle where *two* of its daughters are similar to itself (this is shown as the shaded triangles in Figure 11). In terms of the M_i this means that some permutation of the vector $\mathbf{t} = (\pi/5, 2\pi/5, 2\pi/5)^*$ is an eigenvector associated with eigenvalue 1 for two of the M_i. The only other non-degenerate triangle that also acts as an eigenvector is $T(2\pi/9, \pi/3, 4\pi/9)$ which has *one* of its daughters similar to itself.

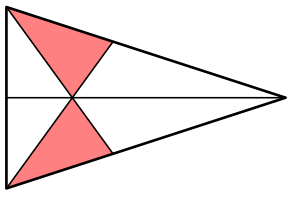

Figure 11: The decomposition of $T(\pi/5, 2\pi/5, 2\pi/5)$.

Figure 10 was computed using random walks and so the distribution is at best approximate. It is not too difficult to find upper and lower bounds for the distribution (though in practice the amount of computation needed to compute these bounds to an accuracy to be able to produce Figure 10 is prohibitive).

The basic idea is to note for a fixed k that $M_{i_1} \cdots M_{i_k}$ maps P into a smaller triangular region of P, let us denote this by Q. So in particular we have that $M_{i_1} \cdots M_{i_k} M_{i_{k+1}} \cdots M_{i_n} \mathbf{t}$ must lie in Q as well for any choice of initial $\mathbf{t}$ and any choice of the $i_{k+1}, \ldots, i_n$. In essence if we know what the last k steps of this Markov process are then we have a lot of information about where in P we end up (the higher the value of k the more precisely we can approximate the point). With this in mind the procedure is to fix a value of k and then look at the image of P under each of the 6^k possible combinations of $M_{i_1} \cdots M_{i_k}$. Now divide the interval between 0 and $\pi/3$ in some fashion. For each interval a lower bound for the distribution is found by counting the number of images Q which *must* have smallest angle in that interval divided by 6^k; an upper bound is found by counting the number of images of Q which *can* have some smallest angle in the interval divided by 6^k. An example of the resulting bounds on the distribution is shown for $k = 15$ and the interval split into widths of $\pi/256$ in Figure 12.

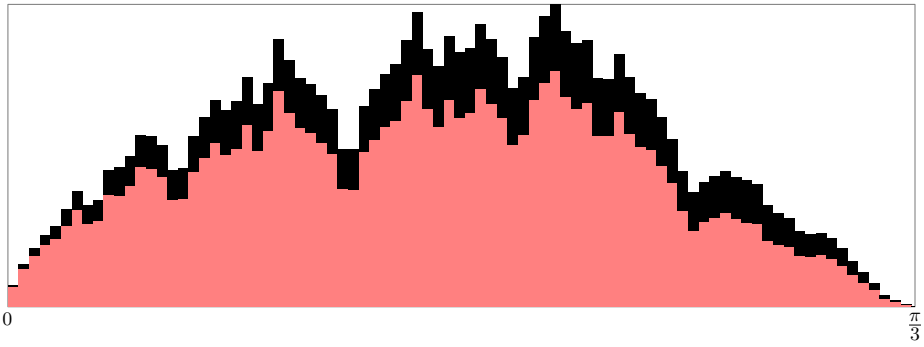

Figure 12: Upper (black) and lower (red) bounds for the true distribution of smallest angle.

The precise location of the peaks and valleys is in general not well understood. For comparison we also include the distribution of the middle and largest angles in Figures 13 and 14 computed in the same way as Figure 10.

3 Subdividing by medians

We now consider the subdivision using the median point of the triangle. We will restrict our attention to the case of six daughters. This case has been well studied because of its close relationship to barycentric subdivision. We will see that this situation is quite different from the case of the incenter. One major difference is that the median map is not contracting on P as we saw previously. In Figure 15 we indicate how one of the median daughters maps P to itself (the other five are similar and differ by rotation and reflections).

To get some intuition about what is happening in this case let us consider the histogram

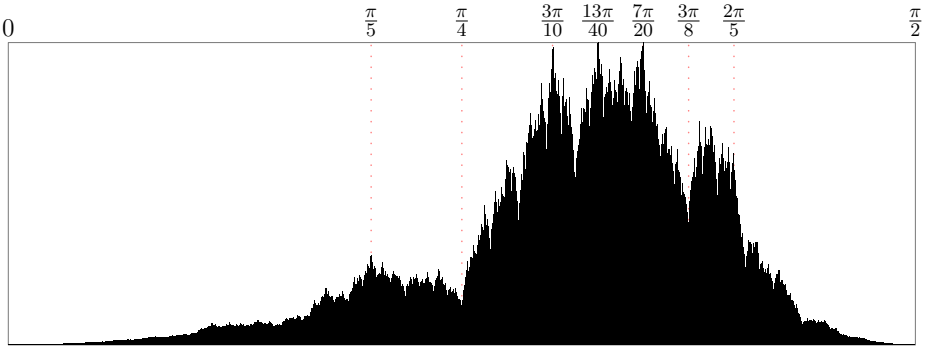

Figure 13: The distribution of the middle angle using bisectors.

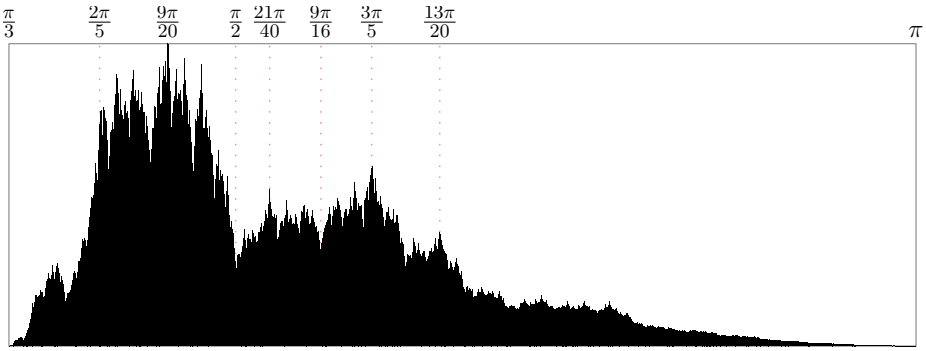

Figure 14: The distribution of the largest angle using bisectors.

for $T(\pi/3, \pi/3, \pi/3)$ for $n = 4, 6, 8, 10$ shown in Figure 16.

Looking at these pictures what seems to be happening is that the triangles in P tend to go towards the vertices as n increases. Or in other words, the triangles are becoming "flat", or nearly colinear, as n gets large. This behavior was first pointed out to us by David Blackwell [4], independently Bárány et al. [2, 15], inspired by a question of Stakhovskii about the distribution of shapes of triangles, showed that most triangles are flat.

3.1 Analytic approach

Blackwell started by putting a triangle in a standard position by putting the longest side along the x-axis with vertices at $(0, 0)$ and $(1, 0)$, the third vertex is then put with $y > 0$ and $x \geq 1/2$. Given a triangle T in standard position we now define the *pseudo-fatness* of T, denoted $PF(T)$, by $PF(T) = \sqrt{y}(3 - x)$. It should be noted that for a triangle in standard position that $y/2$ is the area of the triangle, so the term $\sqrt{y}$ relates to the area. The term $(3 - x)$ acts as an error correction term.

If $T_1, \ldots, T_6$ are the six daughter triangles of T then Blackwell noted that if the average of the pseudo-fatness of the daughters was small compared to the pseudo-fatness of T for

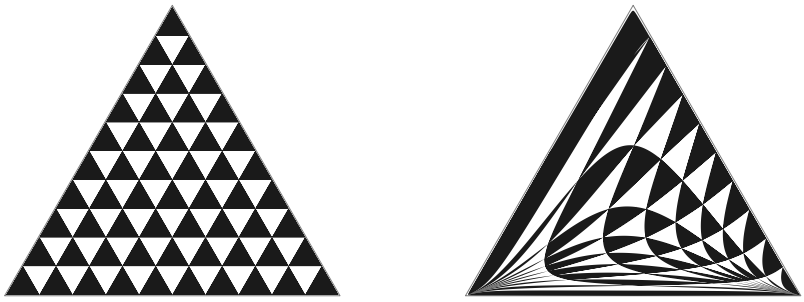

Figure 15: A subdivision of P and its image under the median map.

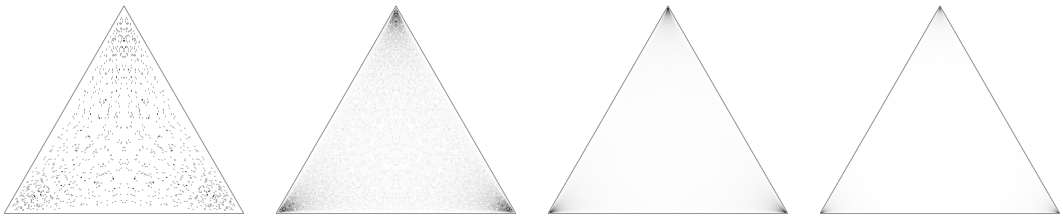

(a) $n = 4$. (b) $n = 6$. (c) $n = 8$. (d) $n = 10$.

Figure 16: The nth generation daughters for medians with six daughters at each generation.

each triangle T, i.e.,

$$\frac{1}{6}\sum_{T_i} PF(T_i) \leq c\, PF(T)$$

for all T and some $c < 1$, then most of the triangles will have pseudo-fatness going to zero. In particular, most of the triangles would be flat.

Computation using Maple confirms this assertion for the value $c = 0.99$ as we show in Figure 17. From this, for example, it would follow that the number of nth generation daughters with smallest angle greater than 0.99^n radians is at most 5.9^n. However, at present no one has confirmed analytically that the above inequality is valid with this value of c. Also it would be interesting to find the best pseudo-fatness function.

There are weaknesses in this approach. Namely, while we can show that the smallest angle is small, this does not automatically imply that the largest angle is large ($\approx \pi$). Or put another way, this approach shows that the triangles drift to the edges of P but not necessarily to the vertices of P. Robert Hough [8] using a different technique was able to show that the largest angle does in fact approach π and moreover gave asymptotic bounds for the proportion of triangles with angles near π, this shows that the triangles do accumulate at the vertices of P.

3.2 Hyperbolic approach

The method of Bárány et al. was to move the problem from P to the hyperbolic half plane. The following approach is similar to theirs and was discovered independently by

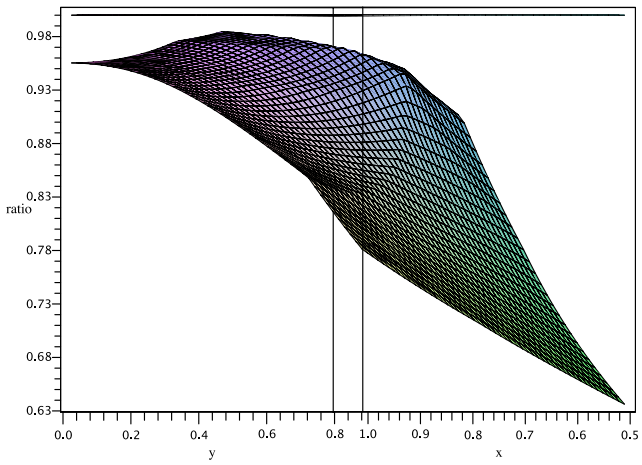

Figure 17: Average of the pseudo-fatness of daughter triangles, seen from the side.

Curt McMullen [14]. The first step is to associate with each triangle T (up to) six points z in the hyperbolic upper half plane $\mathbb{H}$ as shown in Figure 18. Namely, *some* edge of T is located with vertices at $z = 0$ and $z = 1$ and the third vertex is located at the complex coordinate z with positive imaginary part. McMullen then observes that reflecting z across the three circles $\Re(z) = \frac{1}{2}$, $|z| = 1$, and $|z - 1| = 1$ induces a natural action of S_3 on $\mathbb{H}$ in which all six orientations of T occur.

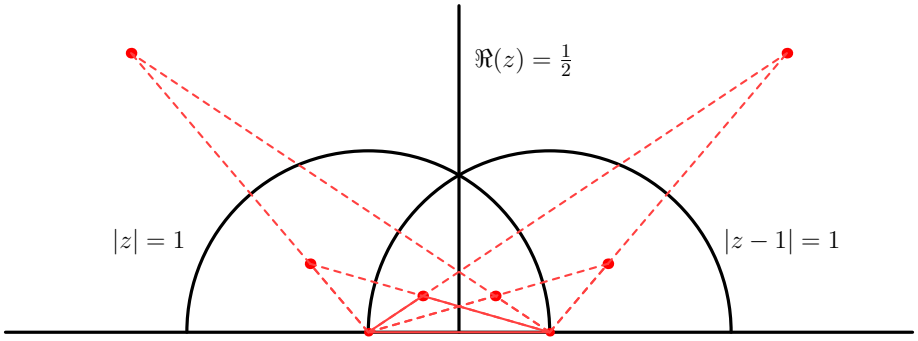

Figure 18: Triangles as points in the hyperbolic plane.

Now, the centroid point of a triangle in this position is represented by the point $(z+1)/3$, and so one of the corresponding daughters becomes $2(z+1)/3$ when normalized. The group of automorphisms of $\mathbb{H}$ generated by the map $B(z) = 2(z+1)/3$ and S_3 is dense in $Aut(\mathbb{H})$ (see [2]). From this, using results of Furstenberg [7], it follows that almost all random walks formed from products of $B(z)$ and elements of S_3 tend to infinity (in the hyperbolic plane) as the length of the product increases. This then implies that almost all of the nth generation daughters have smallest angle tending to 0 as n increases. Actually more can be said in that these points are dense in the hyperbolic space and so every triangle is arbitrarily

"close" so some descendant of the starting triangle.

4 Subdividing by the Gergonne point

We again restrict ourselves to the case of six daughters. The Gergonne point of a triangle is the point of concurrence of the three line segments joining each vertex of the triangle to the point of tangency of the inscribed circle to the side opposite the vertex. We show an example of this in Figure 19, where G denotes the Gergonne point. (As a side note the example shown is the only triangle (up to similarity) with the equilateral triangle as one of the daughters; its side lengths are proportional to 19, 40 and 49, see [5].)

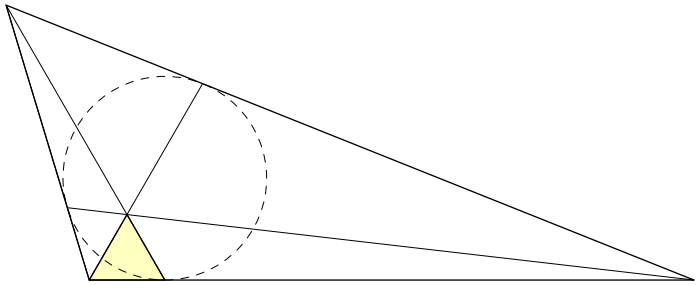

Figure 19: A triangle and its Gergonne point G.

In Figure 20 we look at how one of the Gergonne daughters maps P to itself. It is interesting to note that unlike the medians or angle bisectors this map is not 1-to-1. That is, there is a small region which gets mapped 2-to-1.

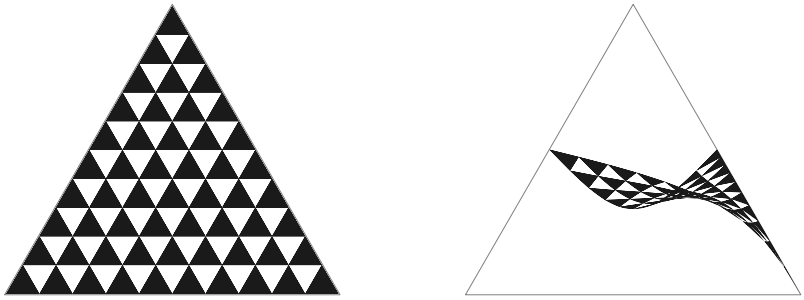

Figure 20: A subdivision of P and its image under the Gergonne map.

Looking at Figure 20 it also looks like the map might be contracting (this would then imply a limiting distribution). However this is not the case. For instance if we consider the following two triangles in the corner $T_1(170°, 5°, 5°)$ and $T_2(160°, 10°, 10°)$ then two of their corresponding daughters are respectively $DT_1(170.0377\ldots°, 9.9245\ldots°, 0.0377\ldots°)$ and $DT_2(160.2935\ldots°, 19.4129\ldots°, 0.2935\ldots°)$. So $\|DT_1 - DT_2\|/\|T_1 - T_2\| = 1.1106\ldots$ showing that there is a slight expansion in the corner. This does not rule out a limiting distribution (and the authors do believe that a limiting distribution exists) it only shows that more sophisticated techniques will be needed.

In Figure 21a we have drawn the histogram for the tenth generation daughters (higher generation daughters seem to have a similar structure). There appears to be a fair amount of white, this is caused not by there being very few triangles in the region, but *no* triangles in the region. In Figure 21b we have darkened the histogram by making any region with a daughter black and any region without a daughter white. As the figure indicates there seems to be large regions with missing daughters. It would be interesting to know what triangles are possible for the nth generation (this is not even known precisely for the first generation).

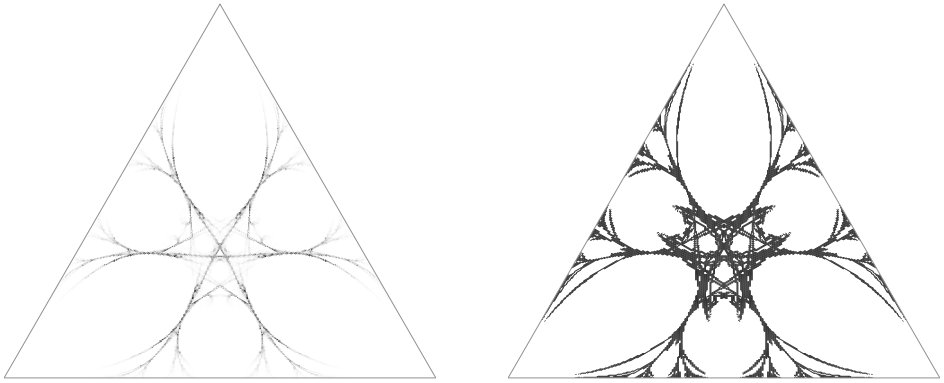

(a) Histogram. (b) Darkened.

Figure 21: The tenth generation daughters for the Gergonne point with six daughters at each generation.

In Figure 22 we indicate the distributions for the middle and largest angles using the Gergonne point divison. Looking at the distributions it seems that the middle angle is concentrated around $\pi/3$ while the largest angle has some approximate symmetry around $\pi/2$. For the largest angle what appears to be happening is that for "most" triangles when using the Gergonne point the largest angles of the daughters are located at the vertex along the edge of the parent triangle. So by pairing up adjacent daughters along the edge their two largest angles should be symmetric around $\pi/2$.

5 Subdividing by the Lemoine point

The Lemoine point of a triangle is the intersection of the symmedians which are the medians reflected across the angle bisectors, so it is also known as the symmedian point. This point seems to be similar to the medians in that the smallest angles go to 0 but experimentally the triangles seem to be going to the *sides* of P rather than the *corners* of P. Further, they seem to be drifting *slowly*. In Figure 23a we have plotted the histogram for all the 10th generation daughters while Figure 23b was formed by random walks of length 30 using the Lemoine point to subdivide.

In Figure 24 we look at how one of the Lemoine daughters maps P to itself. Clearly the map is not contracting. It is also difficult to see what is happening on the left hand side,

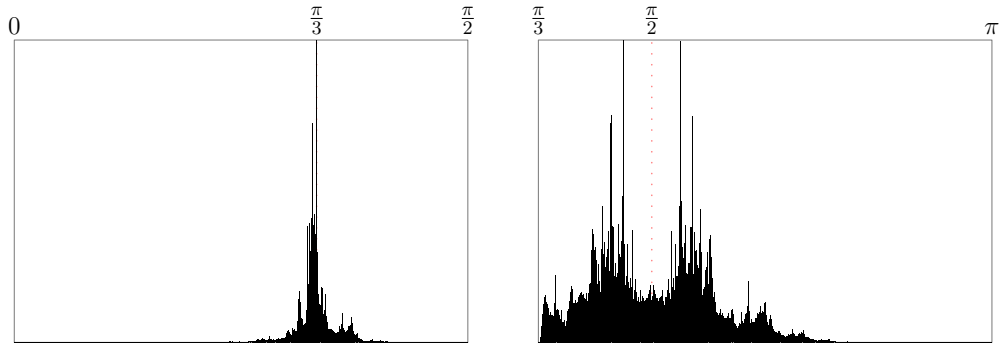

(a) Middle angle. (b) Largest angle.

Figure 22: The distribution of angles using the Gergonne point.

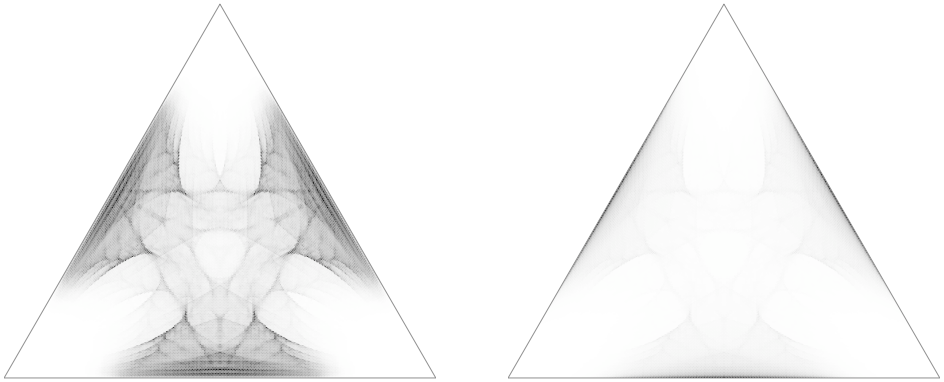

(a) $n = 10$. (b) $n = 30$.

Figure 23: The nth generation daughters for the Lemoine point with six daughters at each generation.

this is because there is a region which gets mapped 3-to-1 onto. It would be interesting to know more about this mapping, for instance where is the folding occurring (experimentally it seems to be folding near the preimage point of $T(\pi/3, \pi/3, \pi/3)$).

6 Concluding Remarks

There are still a large number of questions yet to be answered. For instance, what can be said about the limiting distribution when using bisectors? Is there a limiting distribution when using the Gergonne point, if so what is it? What triangles are missed when P is mapped to itself using the Gergonne daughters? What is the behavior as n tends to infinity when using the Lemoine point? If the triangles are becoming flat what can be said about the rate of convergence?

When looking at the medians we were interested in how the two smallest angles com-

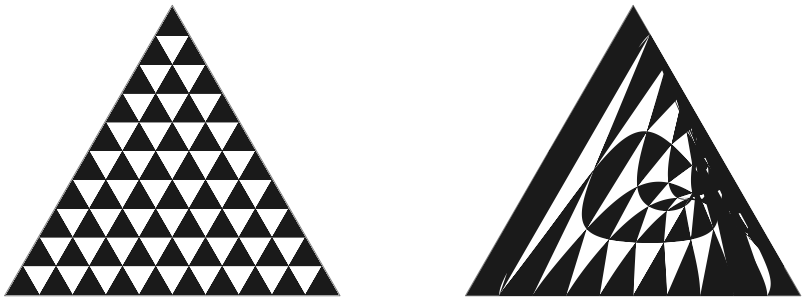

Figure 24: A subdivision of P and its image under the Gergonne map.

pared. When looking at the square of the smallest angle divided by the second smallest angle (giving a ratio between 0 and 1) we got the histogram in Figure 25 divided into 5000 slots; 13611504/17702781 went into the first slot and so we removed that extreme case. The remaining data showed spikes in unusual places, which seem to be connected to the Farey fractions. Is there any explanation for this behavior?

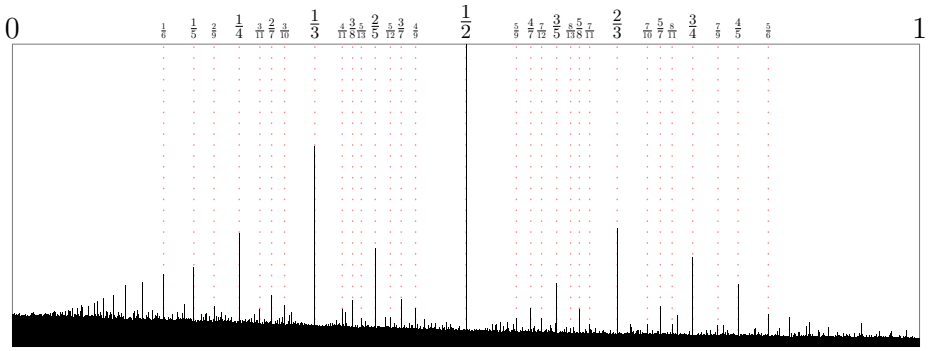

Figure 25: The square of the ratio of the smallest and middle angles using 4091277 random walks with medians of depth 300.

In addition, there is of course a vast catalogue of additional points that can be considered (see [9]). One can also consider variations such as alternating between bisectors and medians at each stage, or using as a central point the midpoint between the incenter and centroid. A much more general question would be to ask what characterizes points where in the limit most triangles are not flat?

One could also consider the problem of where we pick the point uniformly at random in each daughter. In this direction Mannion [12, 13] has shown that if we choose all three vertices at random in the triangle then almost surely the limiting process is collinear.

Similar questions can be asked for higher dimensional analogues. For example Schwartz [18, 19] looked at the distribution of "shapes" when n-simplices are recursively subdivided using Barycentric subdivision. In that case he showed that the behavior is similar to the case of division of triangles using the centroid. It would be interesting to see if there were other well defined points in simplices which generate different behavior (i.e., similar to that

of the incenter or Gergonne points).

Beyond the intrinsic curiosity of these iterated triangle partitions there is also a vast literature on how to subdivide triangles so that the minimal angle is always bounded away from 0 (see [3, 16, 17]). This is desirable since certain methods can fail when the subdivision creates a large number of triangles with minimal angles going to 0 as n gets large. So for instance using medians for subdividing is not desirable since this creates many flat triangles. On the other hand, if we use angle bisectors we can guarantee that all but $f(\varepsilon)$ proportion of the triangles have minimal angles at least ε so that we can limit the proportion of "bad" triangles.

Acknowledgements

We thank David Blackwell for first suggesting these problems to us and Persi Diaconis and Curt McMullen for many useful discussions and insights. We also thank the referee for directing us to related literature.

References

[1] J. C. Alexander, *The symbolic dynamics of pedal triangles*, Math. Mag. **66** (1993), 147–158.

[2] Imre Bárány, Alan F. Beardon and Thomas Keith Carne, *Barycentric subdivision of triangles and semigroups of Möbius maps*, Mathematika **43** (1996), 165–171.

[3] Marshall Bern and David Eppstein, "Mesh generation and optimal triangulation" in *Computing in Euclidean Geometry* Ding-Zhu Du and Frank Hwang, eds. (1992), 23–90.

[4] David Blackwell, personal communication.

[5] Steve Butler, *The lost daughters of Gergonne*, to appear in Forum Geometricorum.

[6] Persi Diaconis and David Freedman, *Iterated random functions*, SIAM Review **41** (1999), 45–76.

[7] Harry Furstenberg, *Noncommuting random products*, Trans. Amer. Math. Soc. **108** (1963), 377–428.

[8] Robert Hough, personal communication.

[9] Clark Kimberling, Encyclopedia of Triangle Centers
`http://faculty.evansville.edu/ck6/encyclopedia/ETC.html`

[10] John Kingston and John Synge, *The sequence of pedal triangles*, Amer. Math. Monthly **95** (1988), 609–620.

[11] Peter Lax, *The ergodic character of sequences of pedal triangles*, Amer. Math. Monthly **97** (1990), 377–381.

[12] David Mannion, *Convergence to collinearity of a sequence of random triangle shapes*, Adv. Appl. Prob. **22** (1990), 831–844.

[13] David Mannion, *The invariant distribution of a sequence of random collinear triangle shapes*, Adv. Appl. Prob. **22** (1990), 845–865.

[14] Curt McMullen, personal communication.

[15] Andrei A. Ordin, *A generalized barycentric subdivision of a triangle, and semigroups of Möbius transformations*, Russian Math. Surveys **55** (2000), 591–592.

[16] María-Cecilia Rivar and Gabriel Iribarren, *The 4-triangles longest-side partition of triangles and linear refinement algorithms*, Math. of Computation **65** (1996), 1485–1502.

[17] Ivo Rosenberg and Frank Stenger, *A lower bound on the angles of triangles constructed by bisecting the longest side*, Math. of Computation **29** (1975), 390–395.

[18] Richard Evan Schwartz, *The density of shapes in three-dimensional barycentric subdivision*, Discrete Comput. Geom. **30** (2003), 373–377.

[19] Richard Evan Schwartz, *Affine subdivision, steerable semigroups, and sphere coverings*, Pure and Applied Mathematics Quarterly **3** (2007), 897–926.